

Low Gilbert damping in Bi/In-doped YIG thin films with giant Faraday effect

Jin Zhan(湛劲), Yi Wang(王一), Xianjie Wang(王先杰), Hanxu Zhang(张晗旭), Senyin Zhu(朱森寅), Lingli Zhang(张伶莉), Lingling Tao(陶玲玲), Yu Sui(隋郁), Wenqing He(何文卿), Caihua Wan(万蔡华), Xiufeng Han(韩秀峰), V. I. Belotelov, and Bo Song(宋波)

Citation: Chin. Phys. B, 2024, 33 (**10**): 107505. DOI: 10.1088/1674-1056/ad6b84
Journal homepage: http://cpb.iphy.ac.cn; http://iopscience.iop.org/cpb

What follows is a list of articles you may be interested in

Skyrmion motion induced by spin-waves on magnetic nanotubes

Tijjani Abdulrazak, Xuejuan Liu(刘雪娟), Zhenyu Wang(王振宇), Yunshan Cao(曹云姗), and Peng Yan(严鹏)
Chin. Phys. B, 2024, 33 (**10**): 107504. DOI: 10.1088/1674-1056/ad5d64

Magnonic band-pass and band-stop filters with structurally modulated waveguides

Lai-He Feng(冯来和), Mang-Yuan Ma(马莽原), Zhi-Hua Liu(刘智华), Kai-Le Xie(解凯乐), and Fu-Sheng Ma(马付胜)
Chin. Phys. B, 2023, 32 (**6**): 067503. DOI: 10.1088/1674-1056/ac8afb

Nonlinear three-magnon scattering in low-damping $La_{0.67}Sr_{0.33}MnO_3$ thin films

Yuelin Zhang(张跃林), Lutong Sheng(盛路通), Jilei Chen(陈济雷), Jie Wang(王婕), Zengtai Zhu(朱增泰), Rundong Yuan(袁润东), Jingdi Lu(鲁京迪), Hanchen Wang(王涵晨), Sijie Hao(郝思洁), Peng Chen(陈鹏), Guoqiang Yu(于国强), Xiufeng Han(韩秀峰), and Haiming Yu(于海明)
Chin. Phys. B, 2023, 32 (**10**): 107505. DOI: 10.1088/1674-1056/acedf8

Observation of nonlinearity and heating-induced frequency shifts in cavity magnonics

Wei-Jiang Wu(吴维江), Da Xu(徐达), Jie Qian(钱洁), Jie Li(李杰), Yi-Pu Wang(王逸璞), and Jian-Qiang You(游建强)
Chin. Phys. B, 2022, 31 (**12**): 127503. DOI: 10.1088/1674-1056/ac9b02

Experimental observation of interlayer perpendicular standing spin wave mode with low damping in skyrmion-hosting $[Pt/Co/Ta]_{10}$ multilayer

Zhen-Dong Chen(陈振东), Mei-Yang Ma(马眉扬), Sen-Fu Zhang(张森富), Mang-Yuan Ma(马莽原), Zi-Zhao Pan(潘咨兆), Xi-Xiang Zhang(张西祥), Xue-Zhong Ruan(阮学忠), Yong-Bing Xu(徐永兵), and Fu-Sheng Ma(马付胜)
Chin. Phys. B, 2022, 31 (**11**): 117501. DOI: 10.1088/1674-1056/ac7bf9

Low Gilbert damping in Bi/In-doped YIG thin films with giant Faraday effect

Jin Zhan(湛劲)[1], Yi Wang(王一)[1], Xianjie Wang(王先杰)[1,5,6,†], Hanxu Zhang(张晗旭)[1], Senyin Zhu(朱森寅)[1], Lingli Zhang(张伶莉)[1], Lingling Tao(陶玲玲)[1], Yu Sui(隋郁)[1], Wenqing He(何文卿)[2], Caihua Wan(万蔡华)[2], Xiufeng Han(韩秀峰)[2], V. I. Belotelov[3], and Bo Song(宋波)[4,5,6,‡]

[1] *School of Physics, Harbin Institute of Technology, Harbin* 150001, *China*
[2] *Beijing National Laboratory for Condensed Matter Physics, and Institute of Physics, Chinese Academy of Sciences, Beijing* 100190, *China*
[3] *Russian Quantum Center, Moscow* 119991, *Russia*
[4] *National Key Laboratory of Science and Technology on Advanced Composites in Special Environments, Harbin Institute of Technology, Harbin* 150001, *China*
[5] *Zhengzhou Research Institute, Harbin Institute of Technology, Zhengzhou* 450046, *China*
[6] *Frontiers Science Center for Matter Behave in Space Environment, Harbin Institute of Technology, Harbin* 150001, *China*

(Received 21 May 2024; revised manuscript received 15 July 2024; accepted manuscript online 6 August 2024)

Magnetic films with low Gilbert damping are crucial for magnonic devices, which provide a promising platform for realizing ultralow-energy devices. In this study, low Gilbert damping and coercive field were observed in Bi/In-doped yttrium iron garnet (BiIn:YIG) thin films. The BiIn:YIG (444) films were deposited onto different substrates using pulsed laser deposition. Low coercivity (<1 Oe) with saturation magnetization of 125.09 emu/cc was achieved along the in-plane direction of BiIn:YIG film. The values of Gilbert damping and inhomogeneous broadening of ferromagnetic resonance in BiIn:YIG films were obtained to be as low as 4.05×10^{-4} and 5.62 Oe, respectively. In addition to low damping, the giant Faraday rotation angles (up to 2.9×10^4 deg/cm) were also observed in the BiIn:YIG film. By modifying the magnetic structure and coupling effect between Bi^{3+} and Fe^{3+} of Bi:YIG, doped In^{3+} plays a key role on variation of the magnetic properties. The low damping and giant Faraday effect made the BiIn:YIG film an appealing candidate for magnonic and magneto-optical devices.

Keywords: magnonic device, Gilbert damping, Faraday effect

PACS: 75.70.Ak, 78.20.Ls, 75.50.Gg, 75.75.–c **DOI:** 10.1088/1674-1056/ad6b84

1. Introduction

Magnonic devices have attracted considerable interests in recent years and are promising as data carriers in next-generation information processing devices, where magnons serve as carrier of spins inside the magnetic materials. Magnons, which are the quanta of spin waves, can efficiently carry spin information without movement of charge during its transmission. As a result, magnonic devices can circumvent the occurrence of Joule heating. Zhang *et al.* theoretically predicted that the magnon can be excited via the s–d exchange interaction between the conduction electrons in the heavy metal (HM) and the localized magnetic moments in the magnetic insulator (MI) due to the magnon-assisted electric current drag phenomenon.[1,2] Han *et al.* experimentally detected and quantitatively verified the $Y_3Fe_5O_{12}$ (YIG) magnetic insulator in a typical HM/MI/HM sandwich structure. They further developed two prototype devices, namely the magnon valves (i.e., YIG/Au/YIG & YIG/Pt/YIG)[3] and the magnon junctions (i.e., YIG/NiO/YIG & YIG/CoO/YIG).[4,5] A novel magnon nonlocal spin Hall magnetoresistance (MNSMR) effect was further discovered and observed in the YIG/NiO/YIG/Pt magnon junction, revealing the transport nature of the magnon as an intermediary.[6] In magnetic materials, the phenomenon of voltage generation driven by temperature gradients in the flow of spins is referred to the spin Seebeck effect (SSE). Due to the fact that SSE does not generate Joule heating from the directed movement of electrons, it has become a focal point in spintronics research in recent years. The strong spin–orbit coupling of Pt and the low damping of YIG makes Pt/YIG the primary focus of research on driving spin currents.[7–9] When Bi_2Se_3 is used as an intermediate layer, the enhancement of surface magnetization is observed, significantly improving SSE of Pt/YIG.[10]

Low Gilbert damping and inhomogeneous broadening of MI are crucial due to the ability of magnon spin currents to propagate and interact effectively with local magnetic textures of MI. YIG film is considered to be an ideal magnon carrier having a long magnon decay length because the values of damping and inhomogeneous broadening are as low as 10^{-5} and 4 Oe, respectively.

Bi-doped YIG is particularly noteworthy in the domains of spintronics and magnonics because of its stronger spin orbit coupling and magneto-optical properties. A lot of researchers

†Corresponding author. E-mail: wangxianjie@hit.edu.cn
‡Corresponding author. E-mail: songbo@hit.edu.cn

© 2024 Chinese Physical Society and IOP Publishing Ltd

have adopted the approach of doping YIG with Bi^{3+} to enhance the Faraday rotation. When the Bi^{3+} replaces Y^{3+} in YIG, the Faraday rotation of YIG is significantly improved, and Bi:YIG exhibits giant Faraday effect.[11–14]

In addition, a large number of studies on magnonic devices focus on Bi:YIG films. Very recently, Fan *et al.* provided evidence that the magnon spin current can drive domain-wall motion in a Bi-doped YIG device by means of magnon spin-transfer torque, and the required energy for driving the domain-wall motion is orders of magnitude less than that required for metallic systems.[15] Caretta *et al.* observed ultrafast domain wall motion using pure spin currents resulting from the spin Hall effect in Bi-doped YIG.[16] Furthermore, the spin current can be driven by a temperature gradient as a result of the spin Seebeck effect in Bi-doped YIG.[17] Many other studies devoted to the development of magnetron devices have been published.[18–20] In the Pt/Bi:YIG bilayer structure, an exponential increase in the intensity of propagating spin waves up to 500% at a propagation distance of ten micrometers.[21] The spin wave travel distance is inversely proportional to the Gilbert damping. However, the magnetic coupling that occurs between Bi^{3+} and the octahedral Fe^{3+} of YIG can result in a large damping.

In this paper, we report low Gilbert damping and coercivity in Bi/In-doped YIG (BiIn:YIG) thin films. The values of Gilbert damping and inhomogeneous broadening of ferromagnetic resonance in the in-plane direction of BiIn:YIG films are as low as 4.05×10^{-4} and 5.62 Oe, respectively. Besides low damping, the variation of giant Faraday rotation angles further confirms the magnetic coupling between Bi^{3+} and octahedral Fe^{3+} in the BiIn:YIG film. The doped In^{3+} can modify the magnetic structure and coupling between Bi^{3+} and Fe^{3+}, which changes the magnetic properties of YIG. Our results open up prospects for the incorporation of YIG films in designs of future magnonic and magneto-optical devices.

2. Method and materials

$Y_3Fe_5O_{12}$, $BiY_2Fe_5O_{12}$ (Bi:YIG) and $BiY_2Fe_{4.7}In_{0.3}O_{12}$ (BiIn:YIG) films (70 nm) were deposited on the (111)-oriented garnet substrates, including $Gd_3Ga_5O_{12}$ (GGG) and $Gd_{2.6}Ca_{0.4}Ga_{4.1}Mg_{0.25}Zr_{0.65}O_{12}$ (SGGG), using pulsed laser deposition (PLD).[13,22–24] The target-to-substrate distance was maintained at 4–6 cm. With a repetition rate of 3 Hz, the targets were ablated using an ArF excimer laser ($\lambda = 248$ nm) inside a vacuum chamber. The laser energy was kept at 250 mJ and the film deposition rate was estimated to be around 1 nm/min. The substrate temperature was kept around 973 K with an ambient oxygen pressure of 20 mTorr. The as-prepared films were annealed under argon gas for three hours at 1073 K. The crystal structure of films was identified by x-ray diffraction (XRD) analysis obtained using an X'Pert XRD spectrometer equipped with Ni-filtered Cu K_α radiation.[25] A vibrating sample magnetometer (VSM, EZ-9) was used to characterize DC magnetic properties. The absorption spectra of ferromagnetic resonance (FMR) were measured within a microwave frequency range of 3–11 GHz (MG3692C) in the in-plane direction of the film at room temperature with a magnetic field up to 3.2 kOe. The modulation amplitude and frequency of their field modulation are 2 V and 921 Hz using a lock-in amplifier (SR830), respectively. The Faraday rotation angle under magnetic field was measured using a lab-created system.

3. Results and discussion

Figure 1(a) displays the XRD patterns of the $Y_3Fe_5O_{12}$ (YIG), $BiY_2Fe_5O_{12}$ (Bi:YIG), $BiY_2Fe_{4.7}In_{0.3}O_{12}$ (BiIn:YIG) films, and the substrates. The single crystal diffraction peak of each film is marked in the illustration. Theoretically, the lattice constants of GGG and SGGG are 12.383 Å and 12.480 Å, respectively. Furthermore, the lattice constants of GGG are closer to those of YIG (12.376 Å). The diffraction peaks of different films are located in the (444) orientation, and the diffraction pattern of the substrates reveals a splitting of the main peak (444).

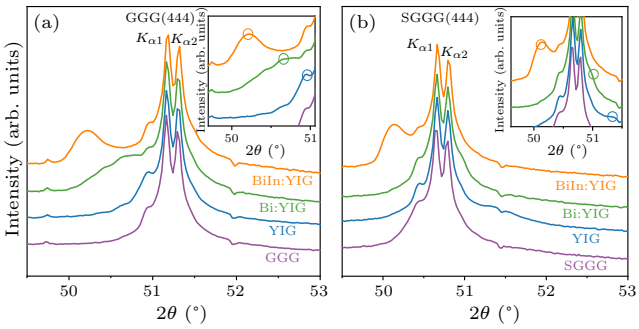


Fig. 1. XRD patterns of YIG, Bi:YIG, and BiIn:YIG films on (a) GGG substrate and (b) SGGG substrate. The diffraction peaks of the films are selectively shown in the inset.

The XRD patterns of films on GGG substrates are also shown in Fig. 1(a), where the single crystal diffraction peaks of YIG, Bi:YIG, and BiIn:YIG are located to the left of the substrate peak. The double peaks for the GGG(444) and SGGG(444) are from the Cu $K_{\alpha1}$ and Cu $K_{\alpha2}$ radiations.[26,27] After the entry of Bi^{3+}/In^{3+} into the lattice, it only influences the lattice constants, but garnet phase still maintains.[28–30] The theoretical lattice constants and lattice mismatches (ε) of YIG, Bi:YIG and BiIn:YIG with GGG, SGGG (111) substrates are listed in Table S1 in the supplementary material. Moreover, as the number of doped-ion species increases, so do the magnitudes of lattice constants, which causes a leftward shift in the diffraction angle. This phenomenon was caused by the variation of the ionic radii, where Bi^{3+} has a larger ionic radius (1.03 Å) than that of Y^{3+} (0.9 Å), and the ionic radius of hexacoordinate In^{3+} (0.8 Å) is larger than that of hexacoordinate Fe^{3+} (0.645 Å). As a result, the films experience com-

pressive strain by the GGG substrate. The XRD patterns of films deposited on the SGGG substrate are shown in Fig. 1(b). The lattice constants of BiIn:YIG films are larger than those of SGGG substrates. Thus, the diffraction peaks of BiIn:YIG films are all located to the left of the substrate and change slightly at GGG and SGGG. The BiIn:YIG films experience compressive strain from the SGGG and GGG substrates. However, the lattice constant of the SGGG substrate is larger than that of YIG and Bi:YIG films, thus diffraction peaks of YIG and Bi:YIG films are positioned to the right of the SGGG substrate, indicating tensile strain on the films. Therefore, the diffraction peaks of Bi:YIG and YIG films clearly exhibit a left shift as the substrate changes from GGG to SGGG. A tensile (compressive) strain will shorten (elongate) the film lattice along the out-of-plane [111] axis for these (111)-oriented YIG-based films, which will affect the magnetic properties of the films.[29]

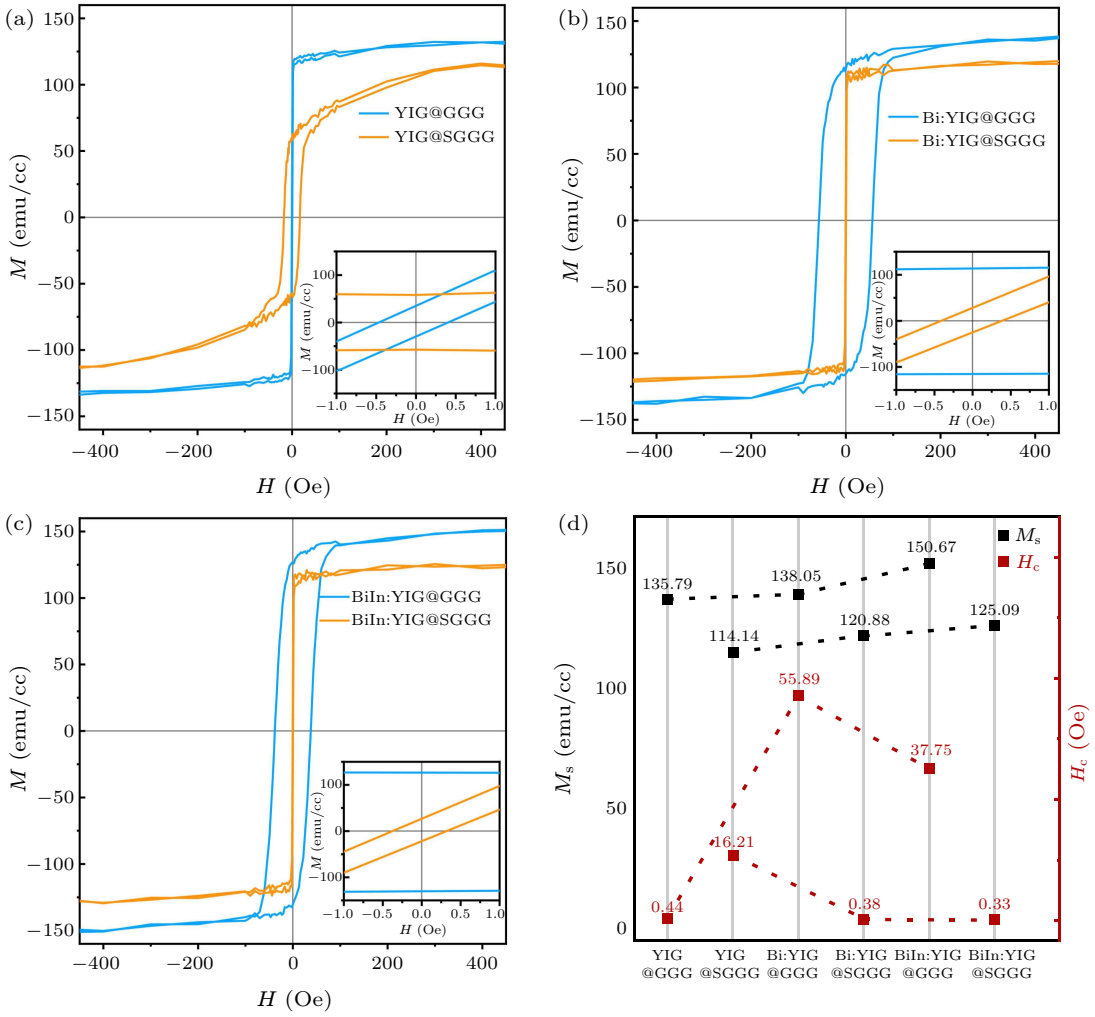


Fig. 2. Magnetic hysteresis loops of films at room temperature. (a)–(c) In-plane magnetic hysteresis loops of YIG, Bi:YIG, and BiIn:YIG on GGG and SGGG substrates, with a close-up view of the curves in the range from −1 Oe to 1 Oe. (d) Numerical plots of saturation magnetization M_s and coercivity H_c for different samples.

The magnetic properties of YIG deposited on GGG and SGGG substrates are illustrated in Fig. 2(a). The (111)-oriented YIG films are found to be magnetically isotropic in-plane, so the influence of in-plane azimuthal angle on magnetism is ignored.[31] It is well-known that there is an antiferromagnetic coupling between Fe^{3+} at the octahedral a-sites and Fe^{3+} at the tetrahedral d-sites in YIG.[32–34] YIG films grown on GGG substrates exhibit significantly lower coercivity (H_c) compared to films on SGGG substrates because the small lattice mismatch between GGG and YIG results in reduced number of defects in YIG films.[35] However, Bi-doped and/or In-doped YIG films exhibit distinct magnetic properties, as shown in Figs. 2(b) and 2(c). In contrast to YIG, the doped films deposited on SGGG substrates have lower H_c (<1 Oe). This is attributed to the larger lattice size of SGGG in comparison to the GGG. Bi:YIG experiences less compressive strain on an SGGG substrate compared to a GGG substrate. Conversely, BiIn:YIG undergoes tensile strain on an SGGG substrate which is opposite to that encountered on a GGG substrate. Based on the above analysis, Bi-doped YIG films grown on SGGG substrates are considered to have a larger ionic radius and a lower H_c. The specific values and trends of

saturation magnetization (M_s) and H_c obtained from different films are demonstrated in Fig. 2(d). The saturation magnetization of YIG@GGG is 137 emu/cc, which is consistent with the previously reported value.[36,37] In comparison to YIG, Bi:YIG exhibits an increase in saturation magnetization.[22] This is ascribed to the magnetic coupling interaction between Bi^{3+} and Fe^{3+} at octahedral *a*-sites, which weakens the magnetic moment of the *a*-site Fe^{3+} and thus enhances the total magnetic moment. Nevertheless, the total magnetic moment of the BiIn:YIG depends on the superposition of the magnetic moments of two different Fe^{3+} positions. Higher M_s and (150.67 emu/cc @GGG, 125.09 emu/cc @SGGG) and lower H_c (37.75 Oe @GGG, 0.33 Oe @SGGG) were observed in BiIn:YIG films. The enhanced M_s observed in BiIn:YIG suggests that the doped In^{3+} ions preferentially occupy the octahedral *a*-sites. Once the non-magnetic In^{3+} ions preferably replace Fe^{3+} ions at the octahedral *a*-sites, the antiferromagnetic coupling between Fe^{3+} ions situated at the octahedral *a*-sites and the tetrahedral *d*-sites weakens which enhances the overall magnetic moment. Usually, the higher the M_s of a material, the stronger its magnetic rotation performance in the microwave frequency range. Ga ions with smaller ionic radius were doped into YIG to reduce the magnetic moment due to its higher probability of occupying the tetrahedral *d*-sites, which results in the reduction of moment.[38] The H_c of the Bi:YIG film is significantly increased due to the large lattice mismatch with the GGG substrate.[39,40] Although there is an increase of lattice mismatch after the co-doping of Bi and In, the replacement of Fe^{3+} at the octahedral *a* site by In reduces the antiferromagnetic coupling between the octahedral *a* site and the tetrahedral *d* site, which is the main reason why the BiIn:YIG exhibits a sudden decrease compared to the Bi:YIG films deposited on the GGG substrate. On the SGGG substrate, the lattice mismatch of Bi:YIG and/or BiIn:YIG is smaller than that on the GGG substrate, so variation of H_c is very small. A low H_c was observed in the BiIn:YIG@SGGG film, which suggests that the BiIn:YIG films can benefit to the transmission of spin waves (magnons) and are more suitable for applications in magnonic devices.

The Landau–Lifshitz–Gilbert (LLG) equation can be used to describe the precession of magnetic moments:

$$\frac{\partial \boldsymbol{M}}{\partial t} = -\gamma \boldsymbol{M} \times \boldsymbol{H}_{\text{eff}} + \frac{\alpha}{M_s} \boldsymbol{M} \times \frac{\partial \boldsymbol{M}}{\partial t}. \tag{1}$$

Here, the first term describes the source of precession, corresponding to the precessional torque of the magnetic moment under an effective magnetic field; γ represents the gyromagnetic ratio. The effective magnetic field is calculated by $H_{\text{eff}} = H_{\text{ex}} + H_{\text{de}} + H_{\text{ani}}$, where H_{ex} represents the exchange field, H_{de} denotes the demagnetization field due to shape anisotropy, $H_{\text{ani}} = 2K_1/M_s$ represents the anisotropy field due to magnetic crystal anisotropy,[41] and K_1 is the anisotropy constant. The second term describes the Gilbert damping torque, with α and M_s being the Gilbert damping and the saturation magnetization, respectively.[42]

The absorption spectra of ferromagnetic resonance (FMR) spanning the microwave frequency range of 3–11 GHz were measured at room temperature, as shown in Fig. 3. The film is placed on the coplanar waveguide (CPW) and the magnetic field along an in-plane direction with the film.[43–45] The ferromagnetic resonance signal was modulated by a coil, which was then detected by a detector equipped with a lock-in amplifier.

The gyromagnetic ratio γ can be achieved by fitting the ground-state YIG formula based on the frequency dependence of the resonance magnetic field (H_{res}):

$$\omega = 2\pi f = \gamma \sqrt{H_{\text{res}}(H_{\text{res}} + 4\pi M_{\text{eff}})}, \tag{2}$$

where ω represents the angular frequency, f is the frequency of the applied microwave field; $4\pi M_{\text{eff}}$ signifies the effective magnetization, $4\pi M_{\text{eff}} = 4\pi M_s - H_{\text{ani}}$; γ represents the gyromagnetic ratio, and the parameter $\gamma/(2\pi)$ of thin film is 2.8 MHz/Oe.[22,26,46–48] By fitting the LLG equation, the frequency-dependent relationship defining the ferromagnetic resonance peak-to-peak linewidth (ΔH_{pp}) could be obtained,[35,45]

$$\Delta H_{\text{pp}} = \Delta H_0 + \frac{2\alpha}{\sqrt{3}\gamma}\omega, \tag{3}$$

where ΔH is the inhomogeneous linewidth.

Table 1. FMR-related parameters involving samples with different compositions.

Sample	Gilbert damping (10^{-4})	Inhomogeneous broadening (Oe)	$4\pi M_{\text{eff}}$ (Gs)	H_{ani} (Gs)
Bi:YIG@GGG	15.3 ± 0.56	7.11 ± 0.32	2151.32 ± 56.63	417.41 ± 7.21
Bi:YIG@SGGG	5.34 ± 0.20	3.89 ± 0.23	1733.80 ± 27.79	162.67 ± 1.84
BiIn:YIG@GGG	23.7 ± 0.63	8.43 ± 0.26	2187.57 ± 63.51	265.15 ± 2.36
BiIn:YIG@SGGG	4.05 ± 0.30	5.62 ± 0.12	1734.24 ± 30.26	215.99 ± 1.67
YIG@GGG	6.06 ± 0.32	3.00 ± 0.10	2102.41 ± 47.33	396.89 ± 3.25
YIG@SGGG	5.09 ± 0.23	2.56 ± 0.05	1517.26 ± 30.46	83.63 ± 0.85

The corresponding FMR-related data at this point are presented in Table 1. The important results can be observed. The H_{ani} values of all films are negative, indicating that the films exhibit the in-plane magnetism.

The ΔH_{pp} as a function of the in-plane azimuthal angle at 7 GHz is shown in Fig. S1 in the supplementary material.

The isotropic FMR linewidth in the (111)-oriented BiIn:YIG film was found, which is consistent with recent studies on the ferroresonance anisotropy field.[49]

Field-modulated FMR across the frequency range of 3–11 GHz was measured for fields in the in-plane direction. The local FMR data pertaining to the BiIn:YIG@SGGG film are shown in Fig. 3(a). Zero-field FMR can be realized at 1.6 GHz, which allows for the excitation of coherent magnons and reduces the saturation magnetization. The slope of the ferromagnetic resonance linewidth with respect to the resonance frequency was fitted for six films using Eq. (3), as shown in Fig. 3(b).

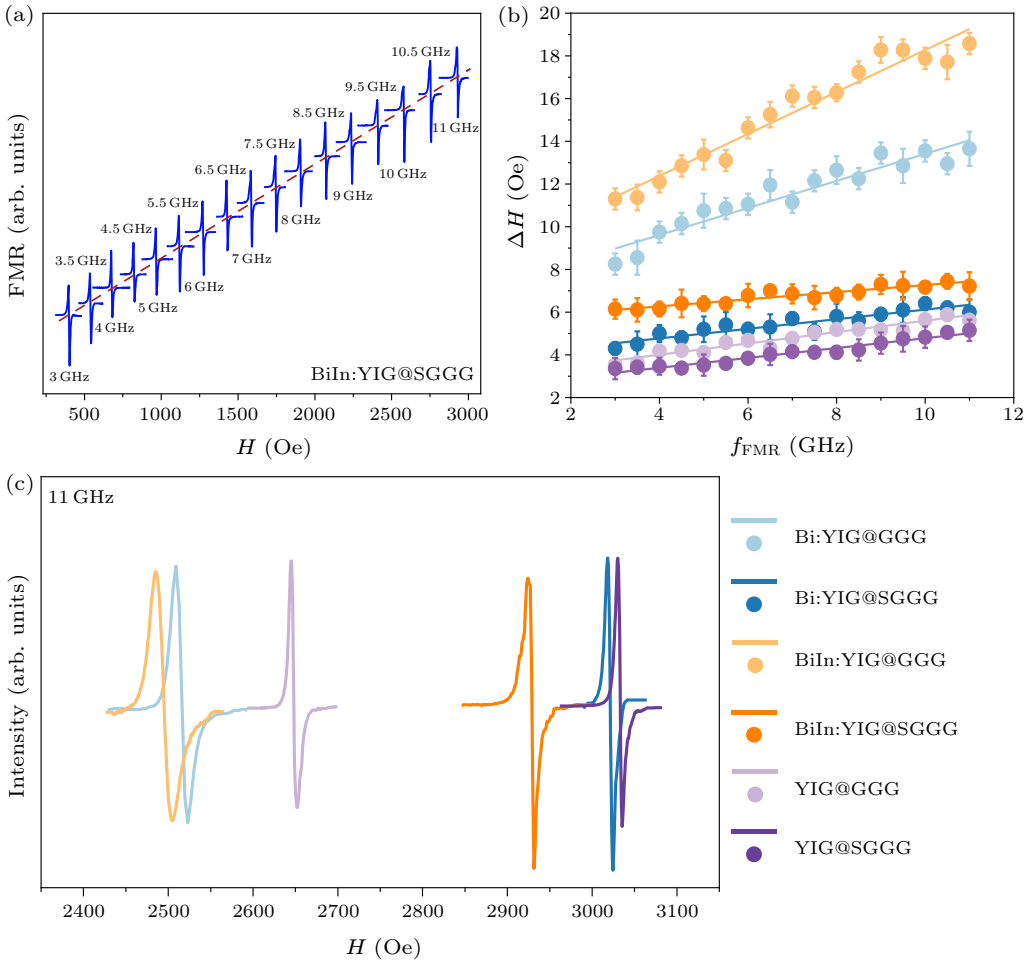


Fig. 3. FMR data of films at room temperature with the magnetic field along the in-plane direction: (a) FMR of the BiIn:YIG film at different frequencies, (b) frequency-dependent fitting results of FMR linewidth ranging from 3 GHz to 11 GHz, (c) FMR signals of films at 11 GHz.

It is worth noting that the BiIn:YIG@SGGG has a low Gilbert damping (4.05×10^{-4}). The Gilbert damping of YIG-based films are shown in Table S2 in the supplementary material. Compared with the metal film, the low damping greatly reduces the power dissipation in the process of magnetism and spread.[15,50] It is well acknowledged that YIG has a lower Gilbert damping, a crucial parameter in the development of magnetism and spintronics. The Gilbert damping of the YIG film deposited on the SGGG substrate was found to be smaller than that on the GGG substrate. The strain is the main factor for the Gilbert damping when the sample has the sample magnetic structure. Although the lattice mismatch between GGG and YIG is smaller than that between SGGG and YIG, but the lattice constants of YIG are smaller than those of the SGGG substrate, the tensile strain can reduce the Gilbert damping. Similar results have been observed in YIG@GGG and YIG@SGGG films.[51] However, the introduction of Bi^{3+} in YIG increases ΔH_{pp} and α on both GGG and SGGG substrates. The inhomogeneous linewidth and Gilbert damping of Bi:YIG are relatively higher. In Bi:YIG films grown on GGG, α increases by an order of magnitude. There are many factors that can affect the Gilbert damping of YIG-based films, including structure, film quality, strain, magnetic moments, interactions between spin and orbit, and so on.[52] However, such phenomena can be explained by the enhanced spin–orbit coupling (SOC) after Bi-doping. Pure YIG exhibits almost quenched orbital momentum of half-filled d shell in Fe^{3+} electron configuration, leads to weak SOC. The coupling between Bi^{3+} and octahedral Fe^{3+} can enhance the spin–orbit coupling which results in a high damping.[53,54] Another reason for the elevated FMR-related parameters is the significant lattice mismatch that exists between the Bi:YIG film and the GGG sub-

strate. The compressive strain imposed by the substrate enhances electron scattering within the lattice.[55] Both lattice constants of YIG and Bi:YIG films are larger than those of the GGG substrate, the compressive strain exerted by the GGG substrate on Bi:YIG is greater than that on YIG, which may enhance the Gilbert damping. The Gilbert damping of the BiIn:YIG film on the SGGG substrate is reduced, because the experiencing compressive strain from the SGGG substrate is smaller than that of GGG. Considering the reduced Gilbert damping by the In-doping and the small compressive strain from SGGG, there is a little reduction of Gilbert damping of BiIn:YIG@SGGG than that of Bi:YIG@SGGG.

The FMR signals of films at 11 GHz are displayed in Fig. 3(c). The YIG films demonstrate the maximum resonance magnetic field, while the BiIn:YIG films show the minimum resonance magnetic field. This is due to the lattice mismatch between the films and the substrate. In the absence of substrate-induced strain and with a small amount of nonmagnetic In^{3+} ions substituting the octahedral Fe^{3+} ions in the crystal, the antiferromagnetic coupling between the *a*-site Fe^{3+} and *d*-site Fe^{3+} reduces. As a result, a lower magnetic field can satisfy the resonance absorption of magnetic moment precession.

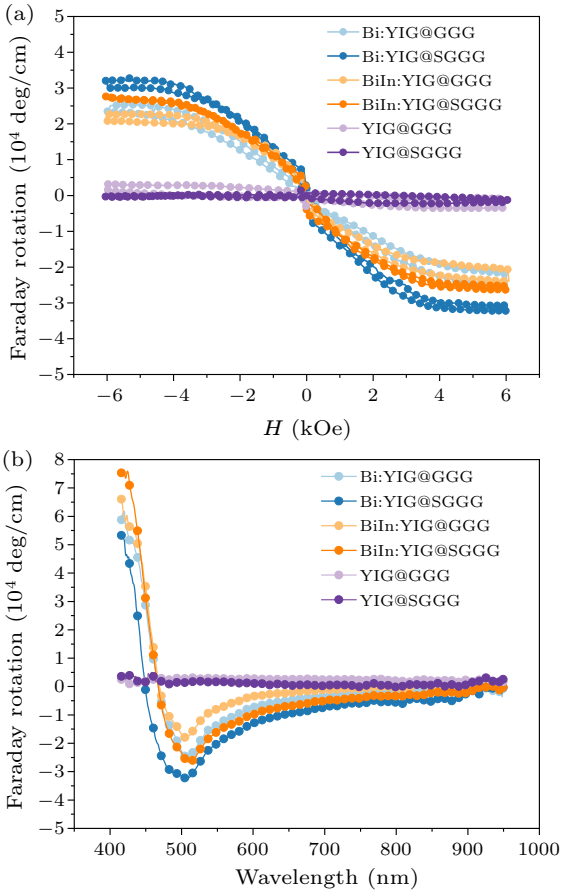


Fig. 4. Faraday effect of YIG, Bi:YIG, and BiIn:YIG films: (a) hysteresis loops under 532 nm laser, (b) Faraday rotation angles within the wavelength range of 40–1000 nm.

The giant Faraday effect has been observed in Bi^{3+}-doped YIG films as a result of the coupling between Bi^{3+} and the octahedral Fe^{3+} ions of Bi:YIG.[56–59] To validate the hypothesis regarding the roles of Bi^{3+} and In^{3+} within the crystal, various Faraday effect tests are presented in Fig. 4. Firstly, we employed light with a wavelength of 532 nm to measure the Faraday rotation angle of the films, since the Faraday effect of the Bi:YIG films at 532 nm has been widely reported.[60–62] Figure 4(a) illustrates the unit-length rotation angle of polarized light subjected to a magnetic field at room temperature. The magnetic field is scanned using a fixed optical wavelength. The light, when directed perpendicular to the plane, passes through the film. Bi:YIG@SGGG exhibits the greatest Faraday rotation angle (3.2×10^4 deg/cm@532 nm), followed by BiIn:YIG@SGGG (2.9×10^4 deg/cm@532 nm). Bi:YIG and BiIn:YIG films on GGG have smaller Faraday rotation angles of 2.5×10^4 and 2.2×10^4 deg/cm@532 nm, respectively. The Faraday rotation angle of the YIG film is much smaller than that of the Bi^{3+}-doped YIG materials. The doped Bi^{3+} ions replace Y^{3+} at the dodecahedron *c*-site, inducing octahedral lattice distortion. The local symmetry of Fe^{3+} in the octahedra is disrupted, leading to an increase in its orbital degeneracy, which amplifies the available energy-level transitions between different excited states and strengthens the oscillator strength of crystal field transitions in the octahedra. This process facilitates and contributes to the enhancement of the Verdet constant via magnetic-optical transitions, particularly within the low-energy region.[56]

When subjected to a fixed magnetic field of 4 kOe, the Faraday rotation angles of all samples attain saturation. The variation of the Faraday rotation angle over different wavelengths is illustrated in Fig. 4(b). The Faraday rotation angles of all films are found to have optical wavelength dependence. However, the wavelength dependence of Faraday rotation angles of Bi:YIG and BiIn:YIG is more pronounced in the same diagram. In addition to this, the sign of the Faraday rotation angle is determined by the direction of the magnetic moment that couples to the electric vector through spin-orbit coupling.[63] The maximal Faraday rotation angle occurs at around 520 nm. Furthermore, the trend of the maximum Faraday rotation angle for several samples correspond to that shown in Fig. 4(a). Obviously, the Faraday rotation angle slightly decreases after In^{3+} doping. The results of the Faraday effect can be interpreted as an evidence supporting that the doped In^{3+} replaces the Fe^{3+} at octahedral *a*-sites of BiIn:YIG because the coupling between Bi^{3+} and octahedral Fe^{3+} of YIG is the source of the giant Faraday effect. Furthermore, the variation of Faraday rotation of $BiY_2Fe_{5-x}In_xO_{12}$ ($x = 0.3, 0.4, 0.5$) films at a wavelength of 532 nm are shown in Fig. S2 in the supplementary material. The Faraday rotation decreases gradually with increasing In content. These results confirm that the doped-In^{3+} ions preferentially occupy the oc-

tahedral *a*-sites and weaken the coupling between Bi^{3+} and octahedral Fe^{3+} in BiIn:YIG.

4. Summary

In conclusion, the structure, magnetic, and Faraday effect of BiIn:YIG films have been investigated in detail. The doped In^{3+} can tune the magnetic structure and the coupling effect between Bi^{3+} and Fe^{3+} of BiIn:YIG. The enhancement of saturation magnetization of BiIn:YIG suggests that the doped In^{3+} preferentially occupies the octahedral *a*-sites of Fe^{3+}, which can be confirmed by the variation of giant Faraday rotation angles in BiIn:YIG films. The coercivity of BiIn:YIG is much smaller than that of Bi:YIG, suggesting that the magnetic coupling strength between magnetic domains weakens after In^{3+} doping. The values of Gilbert damping and inhomogeneous broadening of ferromagnetic resonance in the in-plane direction of BiIn:YIG films exhibit minima of 4.05×10^{-4} and 5.62 Oe, respectively. As a result, BiIn:YIG films can benefit to the transmission of spin waves (magnons) and have better applications in magnonic devices. The findings open up prospects for incorporation of YIG films into designs of forthcoming magnonic devices.

Supplementary material

See the supplementary material for the comparison of lattice constant, Faraday rotation, damping coefficients and Faraday rotation for $BiY_2Fe_{5-x}In_xO_{12}$ ($x = 0.3$, 0.4, 0.5) films.

Acknowledgments

This work was supported by the National Key Research and Development Program of China (Grant No. 2023YFE0201000), the National Science Fund for Distinguished Young Scholars (Grant No. 52225201), the National Natural Science Foundation of China (Grant Nos. 52372004 and 52072085), the Fundamental Research Funds for the Central Universities (Grant Nos. 2023FRFK06001 and HIT.BRET.2022001), and Heilongjiang Touyan Innovation Team Program.

References

[1] Zhang S S L and Zhang S 2012 *Phys. Rev. Lett.* **109** 096603
[2] Zhang S S L and Zhang S 2012 *Phys. Rev. B* **86** 214424
[3] Wu H, Huang L, Fang C, Yang B S, Wan C H, Yu G Q, Feng J F, Wei H X and Han X F 2018 *Phys. Rev. Lett.* **120** 097205
[4] Guo C Y, Wan C H, Wang X, Fang C, Tang P, Kong W J, Zhao M K, Jiang L N, Tao B S and Yu G Q 2018 *Phys. Rev. B* **98** 134426
[5] He W, Wu H, Guo C, Wan C, Zhao M, Xing Y, Tang P, Yan Z, Xia J and Yu T 2021 *Appl. Phys. Lett.* **119** 212410
[6] Guo C Y, Wan C H, He W Q, Zhao M K, Yan Z R, Xing Y W, Wang X, Tang P, Liu Y Z and Zhang S 2020 *Nat. Electron.* **3** 304
[7] Wang C, Cao Y, Wang X R and Yan P 2018 *Phys. Rev. B* **98** 144417
[8] Lin W, Chen K, Zhang S and Chien C L 2016 *Phys. Rev. Lett.* **116** 186601
[9] Nozue T, Kikkawa T, Watamura T, Niizeki T, Ramos R, Saitoh E and Murakami H 2018 *Appl. Phys. Lett.* **113** 262402
[10] Hu Y, Weir M P, Pereira H J, Amin O J, Pitcairn J, Cliffe M J, Rushforth A W, Kunakova G, Niherysh K, Korolkov V, Kertfoot J, Makarovsky O and Woodward S 2023 *Appl. Phys. Lett.* **123** 223902
[11] Hansen P, Witter K and Tolksdorf W 1983 *Phys. Rev. B* **27** 6608
[12] Matsumoto K, Sasaki S, Haraga K I, Yamaguchi K, Fujii T and Asahara Y 1992 *J. Appl. Phys.* **71** 2467
[13] Fakhrul T, Tazlaru S, Beran L, Zhang Y, Veis M and Ross C A 2019 *Adv. Opt. Mater.* **7** 1900056
[14] Wittekoek S, Popma T J, Robertson J and Bongers P 1975 *Phys. Rev. B* **12** 2777
[15] Fan Y, Gross M J, Fakhrul T, Finley J, Hou J T, Ngo S, Liu L and Ross C A 2023 *Nat. Nanotechnol.* **18** 1000
[16] Caretta L, Oh S H, Fakhrul T, Lee D K, Lee B H, Kim S K, Ross C A, Lee K J and Beach G S D 2020 *Science* **370** 1438
[17] Kirihara A, Uchida K i, Kajiwara Y, Ishida M, Nakamura Y, Manako T, Saitoh E and Yorozu S 2012 *Nat. Mater.* **11** 686
[18] Fakhrul T, Khurana B, Nembach H T, Shaw J M, Fan Y, Riley G A, Liu L and Ross C A 2023 *Adv. Mater. Interfaces* **10** 2300217
[19] Siegel G, Prestgard M C, Teng S and Tiwari A 2014 *Sci. Rep.* **4** 4429
[20] Kikuchi D, Ishida M, Uchida K, Qiu Z, Murakami T and Saitoh E 2015 *Appl. Phys. Lett.* **106** 082401
[21] Merbouche H, Divinskiy B, Gouéré D, Lebrun R, El Kanj A, Cros V, Bortolotti P, Anane A, Demokritov S O and Demidov V E 2024 *Nat. Commun.* **15** 1560
[22] Soumah L, Beaulieu N, Qassym L, Carrétéro C, Jacquet E, Lebourgeois R, Ben Youssef J, Bortolotti P, Cros V and Anane A 2018 *Nat. Commun.* **9** 3355
[23] Alam M S, Wang C, Chen J, Zhang J, Liu C, Xiao J, Wu Y, Bi L and Yu H 2019 *Phys. Lett. A* **383** 366
[24] Zhou L, Song H, Liu K, Luan Z, Wang P, Sun L, Jiang S, Xiang H, Chen Y and Du J 2018 *Sci. Adv.* **4** eaao3318
[25] Zhang H X, Zhu S Y, Zhan J, Wang X J, Wang Y, Yao T, Mezin N I and Song B 2023 *Chin. Phys. Lett.* **40** 127801
[26] Sun Y, Song Y Y, Chang H, Kabatek M, Jantz M, Schneider W, Wu M, Schultheiss H and Hoffmann A 2012 *Appl. Phys. Lett.* **101** 152405
[27] Liu T, Chang H, Vlaminck V, Sun Y, Kabatek M, Hoffmann A, Deng L and Wu M 2014 *J. Appl. Phys.* **115** 17A501
[28] Nazlan R, Hashim M, Ibrahim I R, Mohd Idris F, Wan Ab Rahman W N, Abdullah N H, Ismail I, Kanagesan S, Abbas Z and Azis R S 2015 *J. Mater. Sci.: Mater. Electron.* **26** 3596
[29] Jia Y, Liang Z, Pan H, Wang Q, Lv Q, Yan Y, Jin F, Hou D, Wang L and Wu W 2023 *Chin. Phys. B* **32** 027501
[30] Yang Q H, Zhnag H W, Wen Q Y, Liu Y L, Ihor M S and Ihor I S 2009 *Chin. Phys. Lett.* **26** 047401
[31] Ibrahim N B, Edwards C and Palmer S B 2000 *J. Magn. Magn. Mater.* **220** 183
[32] Krishnan R 1977 *Appl. Phys. Lett.* **31** 237
[33] Geller S and Gilleo M A 1957 *J. Phys. Chem. Solids* **3** 30
[34] Geschwind S 1961 *J. Appl. Phys.* **32** S263
[35] Gallagher J C, Yang A S, Brangham J T, Esser B D, White S P, Page M R, Meng K Y, Yu S, Adur R and Ruane W 2016 *Appl. Phys. Lett.* **109** 072401
[36] Lin Y, Jin L, Zhang H, Zhong Z, Yang Q, Rao Y and Li M 2020 *J. Magn. Magn. Mater.* **496** 165886
[37] Ding J, Liu C, Zhang Y, Erugu U, Quan Z, Yu R, McCollum E, Mo S, Yang S, Ding H, Xu X, Tang J, Yang X and Wu M 2020 *Phys. Rev. Appl.* **14** 014017
[38] Gilleo M A and Geller S 1958 *J. Appl. Phys.* **29** 380
[39] Hauser C, Richter T, Homonnay N, Eisenschmidt C, Qaid M, Deniz H, Hesse D, Sawicki M, Ebbinghaus S G and Schmidt G 2016 *Sci. Rep.* **6** 20827
[40] Kumar R, Samantaray B and Hossain Z 2019 *J. Phys.: Condens. Matter* **31** 435802
[41] Gurjar G, Sharma V, Patnaik S and Kuanr B K 2021 *Mater. Res. Express* **8** 066401
[42] Petit S, Baraduc C, Thirion C, Ebels U, Liu Y, Li M, Wang P and Dieny B 2007 *Phys. Rev. Lett.* **98** 077203
[43] Kang C, Wang T, Jiang C, Chen K and Chai G 2021 *J. Alloys Compd.* **865** 158903
[44] Wang W, Li P, Cao C, Liu F, Tang R, Chai G and Jiang C 2018 *Appl. Phys. Lett.* **113** 042401
[45] Kalarickal S S, Krivosik P, Wu M, Patton C E, Schneider M L, Kabos P, Silva T J and Nibarger J P 2006 *J. Appl. Phys.* **99** 093909

[46] Kehlberger A, Richter K, Onbasli M C, Jakob G, Kim D H, Goto T, Ross C A, Götz G, Reiss G, Kuschel T and Kläui M 2015 *Phys. Rev. Appl.* **4** 014008
[47] Vasili H B, Casals B, Cichelero R, Macià F, Geshev J, Gargiani P, Valvidares M, Herrero-Martin J, Pellegrin E, Fontcuberta J and Herranz G 2017 *Phys. Rev. B* **96** 014433
[48] Grachev A A, Sheshukova S E, Kostylev M P, Nikitov S A and Sadovnikov A V 2023 *Phys. Rev. Appl.* **19** 054089
[49] Zhao Z, Zhang L, Chen Y, Zhong Z, Tang X, Zhang Y, Zhang H and Jin L 2024 *Appl. Phys. Lett.* **124** 052405
[50] Han J, Zhang P, Hou J T, Siddiqui S A and Liu L 2019 *Science* **366** 1121
[51] Liu Q B, Meng K K, Xu Z D, Zhu T, Xu X G, Miao J and Jiang Y 2020 *Phys. Rev. B* **101** 174431
[52] Hurben M J and Patton C E 1998 *J. Appl. Phys.* **83** 4344
[53] Zenkov A V, Moskvin A S 2002 *J. Phys.: Condens. Matter* **14** 6957
[54] Parchenko S, Stupakiewicz A, Yoshimine I, Satoh T and Maziewski A 2013 *Appl. Phys. Lett.* **103** 172402
[55] Schoen M A W, Thonig D, Schneider M L, Silva T J, Nembach H T, Eriksson O, Karis O and Shaw J M 2016 *Nat. Phys.* **12** 839
[56] Xu K, Zhang L, Godfrey A, Song D, Si W, Zhao Y, Liu Y, Rao Y, Zhang H and Zhou H A 2021 *Proc. Natl. Acad. Sci. USA* **118** e2101106118
[57] Liang X, Xie J, Deng L and Bi L 2015 *Appl. Phys. Lett.* **106** 052401
[58] Crossley W A, Cooper R W, Page J L and Van Stapele R P 1970 *Phys. Rev. B* **1** 4503
[59] Takeuchi H, Shinagawa K and Taniguchi S 1973 *Jpn. J. Appl. Phys.* **12** 465
[60] Alam M N E, Vasiliev M and Alameh K 2014 *Opt. Mater. Express* **4** 1866
[61] Nur-E-Alam M, Vasiliev M and Alameh K 2017 *Opt. Mater. Express* **7** 676
[62] Kuila M, Deshpande U, Choudhary R J, Rajput P, Phase D M and Raghavendra Reddy V 2021 *J. Appl. Phys.* **129** 093903
[63] Dionne G F and Allen G A 1993 *J. Appl. Phys.* **73** 6127